OPTIMAL CONTROL DESIGN FOR MULTITERMINAL HVDC

by

Benoit de Courreges d'Ustou

B.S. in Electrical Engineering, ESIGELEC, 2011

Submitted to the Graduate Faculty of

Swanson School of Engineering in partial fulfillment

of the requirements for the degree of

Master of Science

University of Pittsburgh

2012

UNIVERSITY OF PITTSBURGH

SWANSON SCHOOL OF ENGINEERING

This thesis was presented

by

Benoit de Courreges d'Ustou

It was defended on

November 7, 2012

and approved by

Zhi-Hong Mao, PhD, Associate Professor, Department of Electrical and Computer Engineering

Gregory Reed, PhD, Associate Professor, Department of Electrical and Computer Engineering

Mahmoud El Nokali, PhD, Associate Professor, Department of Electrical and Computer Engineering

William Stanchina, PhD, Chairman and Professor, Department of Electrical and Computer Engineering

Thesis Advisor: Zhi-Hong Mao, PhD, Associate Professor, Department of Electrical and Computer Engineering

Gregory Reed, PhD, Associate Professor, Department of Electrical and Computer Engineering

OPTIMAL CONTROL DESIGN FOR MULTITERMINAL HVDC

Benoit de Courreges d'Ustou, M.S.

University of Pittsburgh, 2012

This thesis proposes an optimal-control based design for distributed frequency control in multi-terminal high voltage direct current (MTDC) systems. The current power grid has become overstressed by rapid growth in the demand for electric power and penetration of renewable energy. To address these challenges, MTDC technology has been developed, which has the potential to increase the flexibility and reliability of power transmission in the grid. Several control strategies have been proposed to regulate the MTDC system and its interaction with connected AC systems. However, all the existing control strategies are based on proportional and integral (PI) control with predetermined controller structures. The objective of the thesis is to first determine if existing control structures are optimal, and if improved controller structures can be developed.The thesis proposes a general framework to determine the optimal structure for the control system in MTDC transmission through optimal feedback control. The proposed method is validated and demonstrated using an example of frequency control in a MTDC system connecting five AC areas.

TABLE OF CONTENTS

LIST OF TABLES

LIST OF FIGURES

1.0 INTRODUCTION

1.1 BACKGROUND

In the past twenty years the number of HVDC (High Voltage Direct Current) installations worldwide has significantly increased. This electrical power transmission technology is composed of four main parts: a rectifier that converts the Alternative Current (AC) to DC, a DC transmission line, a inverter which achieves the conversion back to AC and all the interconnected AC and DC support equipment. The installation can be applied for either one line transmission with one rectifier and one inverter, or a DC grid interconnected through a multiterminal system. In industry, DC technology has started to be widely used to compensate some issues such as the reduction of the power loss within industrial and commercial networks. Several contemporary issues can explain the development of HVDC technology:

• First, the acceleration of the integration of renewable energy, especially wind and solar energy, within the electrical network of developed countries has necessitated the development of solutions that are more reliable and efficient than classic AC technologies. HVDC technology allows a better integration of these renewable energy resources : Its low interaction with the environment, especially in underground and underwater configuration, and its high controllability enable HVDC configurations to be more competitive for the distribution sector.

• Second, the increase in energy needs, especially in the group of countries known as the BRIC (Brazil, Russia, India and China), has necessitated the transport of electrical energy, relatively far from the population center, over long distances. The concept of the break-even

distance, where "*the savings in line costs offsets the higher converter station costs*" [1], appears for the choice between AC or DC technology. For an installation requiring a distance of transmission longer than the break-even distance, HVDC technology is economically more suitable because of its high capacity in terms of energy transmission.

• Third, the expansion of the electrical market within continents has revealed the issues of the poor robustness of the grid and the lack of flexibility in the transmission between areas with different electrical norms. Classical AC technology is efficient as long the as expansion is structured in common standards and norms. HVDC link allows a flexible and secure transmission of the electrical power between synchronous and non-synchronous areas regardless of their standards.

Two different configurations are mainly used nowadays: the first and oldest configuration is the Line Commutated Converter (LCC) HVDC. This technology is based on the thyristor valves which can be turned on by controlaction.It is mostly used for long distance transmission line. The second one is called Voltage Source Converter (VSC) HVDC, instead of the simple thyristor, this technology uses the insulated gate bipolar transistor (IGBT) or the gate turn off thyristor (GTO), controlled through the pulse width modulation (PWM) technique [2].This technology has two degrees of freedom: both trun-on and turn-off can be controlled. This addistional controllability allows VSC HVDC to be used for wind farm integration and passive network supply because active and reactive power can be controlled independently and bidirectionally [3], [4].

The expansion of the DC grid necessitates the reduction of the risk of power failure by spreading it through the grid, with a configuration that ensures a back up system. The multiterminal structure has been proposed and developed to increase the interconnectivity of the HVDC installations, and therefore decrease the risk of black out and power failure in one area. However this configuration is still rarely used.

With the development of the DC grid model the frequency control strategy has appeared to be problematic. In the AC grid model, the frequency is regulated with a three-level frequency control system. The controller ensures a stable value of the frequency using the coordination of the power transmitted between the different AC areas and allows the sharing of the load between each area. The frequency control system assumes that each generator and at a higher level each AC area participate to regulate the total frequency deviation introduced by the variation of the load. For a DC grid, the coordination is compromised [5]. From the AC grid point of view the HVDC terminal acts as an independent power supply [2]. This "disjunction" in terms of frequency between the terminals is one of the challenges for inter-area frequency control system.

1.2 LITERATURE REVIEW

In [6], J. Reeve presented a basic presentation of the multiterminal technology. J. Reeve brings together 17 years of studies about HVDC development conducting a comparative evaluation of the literature references. He also underlines the concept of a centralized power control system to improve the flexibility of multiterminal operations.

Mathematical models of the multiterminal configuration are developed in [7], [8] and [9]: The reference [7] studies the implementation of Newton power flow algorithm for a multi-terminal HVDC system with two different mathematical models. The first model consider the converters are co-located the same substation, which means that the DC network is not considered, the while the second model is generalized with a explicit representation of the DC grid. Reference [8] presents a general mathematical model for VSC HVDC system. The asset of the model is its applicability for any topology of the DC grid. This reference apply the model for a two and six terminals. Finally [9], presents a model adapted for large scale study including the transient mathematical equation of the synchronous generator and the *IEEE type* 1 exciter.

One of the main purposes of the VSC HVDC technology is the integration of wind farms inside the electrical grid. Different installations have been studied in [10], [11] and [12]. In [10] a DC voltage controller including strategies for power dispatch are presented in a multiterminal structure. Normal and AC fault configuration are tested to validate the system. The reference [11] presents three configurations of wind farms integrations. Different control designs are tested to regulate the VSC system. In [12], an hybrid multiterminal HVDC is analyzed as a interconnected system with 5 AC areas.

The issue of the power quality has been also investigated in [13]. It shows that multiterminal are capable to ensure an uninterrupted quality power but it can induce an additional cost due to the use of underground cables.

In reference [2], A. Yazdani and R. Iravani presents the majors VSC HVDC configurations such as STATCOM, back-to-back, grid imposed frequency, and variable speed wind power system. All VSC HVDC systems are detailed with a control model for each configuration. Other classic control strategies have been investigated to regulate a single link HVDC and a multiterminal system. In [14] a voltage margin strategy is used to control the terminals through the Voltage-Power characteristics. In [15] a DC voltage-current droop strategy is applied for a single link. A Master-Slave design is studied in one of the multiterminal HVDC configuration presented in [11]. In [8] a classic inner and outer coupled controllers is developed to regulate the HVDC system.

Various advance strategies have been investigated. In [16], an advanced DC voltage controller is derived and tested under loss of one terminal in the system. In [17] the optimal tracking method and the optimal state regulator are designed and evaluated for a simple HVDC link. In [18] a coordinated controller with two hierarchical levels are derived using the optimal control theory. A decentralized eigenvalue placement technique in [19] is studied and applied for the power modulation of multiterminal HVDC systems.

The classic frequency control system (three levels frequency control) has to be modified if HVDC links are integrated within AC grid. HVDC link allows the interconnection of two AC areas with different frequency standard, *id est* each terminal is autonomous and has an independent frequency controller [3], [4] and [20]. In [3] three different frequency controllers are presented. The first controller correspond to a fixed reference frequency value supplied to the VSC HVDC output voltage. The second controller introduce the reference frequency of the VSC HVDC output voltage from the effectiveness of the DC voltage. The third controller is a Proportional-Integral (PI) regulator based on the active power frequency characteristics [4], [20]. Its input is an estimation of the frequency coming from the Phase Locked Loop (PLL).

The notions of primary reserved shared and optimal communication topology applied in HVDC system have rarely been studied in the past. This problematic is investigated in [5], where a distributed Proportional-Integral frequency control for multiterminal HVDC's interconnected with AC areas with a fixed communication topology is developed. The aim of this control strategy was to share primary reserve of each area based on the *rendez-vous* method [21]. In [22] various physical topologies of multiterminal offshore wind farms are studied then compared under normal and different faults on the DC grid.

1.3 MOTIVATION

A majority of the control methods developed in the literature are looking for the isolation of each sub-system,interconnected by th DC grid, from the frequency point of view.

This configuration allows the connection between non-synchronous sub-systems. Furthermore, the configuration prevents a possible cascade of outages within the grid, which would have lead to a possible black out [5].However, this configuration does not allow each sub-system to share the primary reserve with in the grid. Each sub-systems does not communicate

its frequency excursion to the sub-system interconnected [5]. In a classic AC grid, inter-area communication of the frequency deviation would allow the three levels of the frequency control system to regulate and cancel the deviation through the sharing of the primary reserve of each interconnected sub-system.

From an economic point of view, the primary reserve represent an important operational cost. Therefore, the possibility to share it between areas, synchronous or not, would reduce the final cost of the supply significantly and improve the power-tracking of the HVDC system [5]. Furthermore, knowing a static physical topology of a DC grid in a multiterminal HVDC system, the problem of the optimal communication topology between the sub-system is vital. Indeed, the communications could have a significant impact on the configuration and values of controllers themselves. The possibility to include an optimization process in the configuration of each controller coupled with the communication topology would give us a global optimal distributed control design.

In [5] the purpose is the design of a distributed Proportional-Integral (PI) frequency control scheme applied for five interconnected AC areas through multiterminal system. The communication topology of the DC grid is included in the *rendez-vous* configuration of the controller. However the Proportional and Integral parameters are fixed for each susb-system, so not optimal.

The aim of this thesis is to derive the first step which would allow ultimately the realization of the global optimal distributed controller. A general optimal distributed Proportional-Integral-Derivative (PID) applied for frequency control in a multiterminal HVDC is presented in this research. The control model allows the sharing of the load between the AC areas through the DC grid. The optimization of each parameters is made through a state feedback design. The communication topology is not include in this research. The optimization of the multiterminal system therefore considers a full state feedback optimization. The results are compared with the ones from [5].

2.0 MATHEMATICAL MODEL OF THE POWER SYSTEM

This chapter present the development of mathematical equations expressing the multiterminal system and its interconnections.

2.1 FREQUENCY CONTROL SYSTEM

This section introduces the primary and secondary frequency control, the first two levels of the automatic frequency control for an electrical area.

2.1.1 Primary Frequency Control

The primary frequency control can be considered as a short term (few seconds) local controller. The controller can be at generator or power plant level. The purpose of the primary frequency control is to regulate the electrical frequency output of the generator as close as possible to the frequency reference f^{ref}. By looking at the shaft's rotating speed, which is proportional to the output frequency, and the output power of the generators, and comparing them with the reference values f^{ref} and $P^{\text{ref}}_{\text{mech}}$, the primary control induce an adjustment of the opening valves in order to bring the frequency back to an acceptable value [5].

The primary frequency control dynamic is expressed as :

$$T_{\text{mech}} \frac{\mathrm{d}P_{\text{mech}}}{\mathrm{d}t} = P^{\text{ref}}_{\text{mech}} - P_{\text{mech}} - \frac{P^{\text{ref}}}{\sigma} \frac{f - f^{\text{ref}}}{f^{\text{ref}}} \tag{2.1}$$

with T_{mech} the servomotor's time constant, P_{mech} the mechanical power input of the generator, P^{ref} the rated mechanical power of the generator, σ the generator droop and f the electrical output frequency of the stator of the generator.

The aim of the primary frequency control is not to delete totally the excursion of the frequency f, but to bring it back to an acceptable value as fast as possible. Equation (2.1) reveals that the control law is a pure gain. Therefore, a steady state error will unavoidably remain present in the output frequency of the generator [23].

To delete totally the steady state error, a second loop in the control process is necessary. This loop is called the secondary frequency control.

2.1.2 Second Frequency Control

The second level in the frequency control system is designed to eliminate the steady state error present in the output frequency of the generator. It can be done either manually by an operator or automatically through the Automatic Generating Control (AGC) [23].

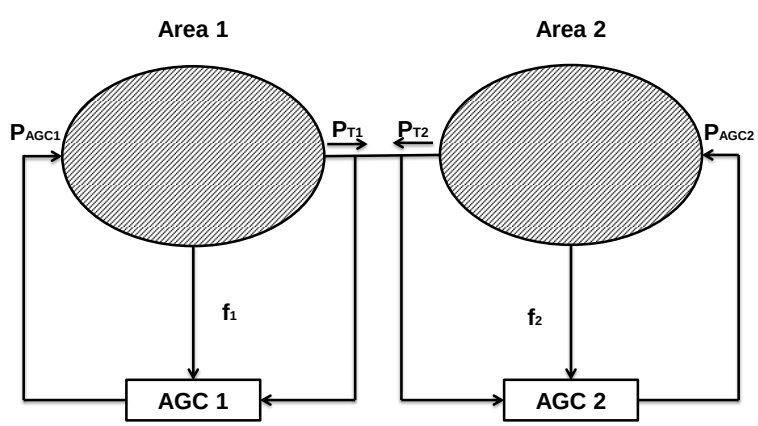

Figure 2.1: Two areas interconnected with the AGC controller.

The secondary frequency control or Load Frequency Control can be synthesized with a Proportional-Integral (PI) controller. Contrary to the primary frequency control its operational place is at the area's level.

For a group of AC areas interconnected, the inputs of the AGC control of one area are the frequency excursion and the power transmitted to the other areas. The power output is then added to the scheduled power and sent to the generators of the areas as the new power reference $P_{\text{mech}}^{\text{ref}}$. This procedure is repeated approximately every 30 s, therefore with a time constant longer than the primary frequency control [5] [23].

It insures not only that the frequency is converging toward f^{ref} but also that the power exchanged between the areas follows the scheduled power transfers.

2.2 INTERCONNECTED SYSTEM

This section introduces the basic mathematical model of the multiterminal HVDC interconnected with AC areas. Assumptions used in this thesis are also presented.

2.2.1 Primary Reserve

Associated with the primary frequency control, the primary control reserves (also known as primary reserve) corresponds to the power margins available to compensate in short period of time the power imbalance detected trough the frequency excursion.

For each generator the mechanical power P_{mech} is bounded by $P_{\text{mech}}^{\text{min}}$ and $P_{\text{mech}}^{\text{max}}$. These limits are due to the technical characteristics of the generator and the economic dispatch of the area [5]. Therefore, the primary reserve is defined as :

$$P_{\text{reserve}} = P_{\text{mech}}^{\text{max}} - P_{\text{mech}}^{\text{ref}}. \tag{2.2}$$

2.2.2 Multiterminal HVDC Model

The system studied in this thesis is a multiterminal HVDC connecting N AC areas (Fig. 2.2). The electrical conversion from AC to DC is made through N converters. Inside of the DC grid, $M \geq N$ nodes are considered such as the node $i, \forall i \in \{1, ..., N\}$ is connected to the AC area i.

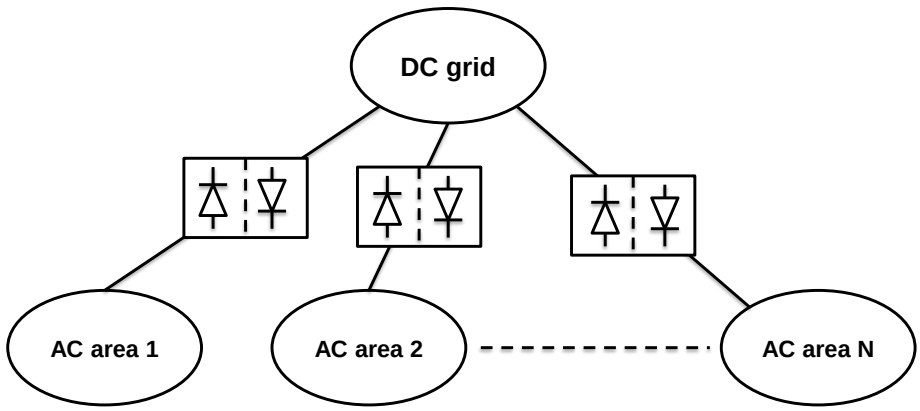

Figure 2.2: Multitermianl HVDC system interconnected with N AC areas.

The power transferred between the node i and j inside of the DC grid is defined as P_{ij}^{dc}. In this thesis only direct and indirect connections between two nodes within the DC grid are considered.

In order to satisfy the power balance within the DC grid, the power injected P_i^{dc} from the AC area i into the DC grid can be define as:

$$\sum_{i \neq j} P_{ij}^{\text{dc}} = \begin{cases} P_i^{\text{dc}} \text{ for } & i \leq N. \\ 0 \text{ for } & i > N. \end{cases} \tag{2.3}$$

Some assumptions can be made from the DC grid characteristics:

In this thesis the time constant of the DC grid is considered much smaller than the AC areas [5]. Therefore the transient dynamics of the DC grid are not considered in this thesis.

Second, the losses inside of the DC grid are considered small compared to the power exchanged inside the grid. Therefore, the DC grid is considered lossless, which means that all the power injected from some AC Areas into the DC grid has to go out into the other AC areas without losses. In another word :

$$\sum_{i=1}^{N} P_i^{\mathrm{dc}} = 0. \tag{2.4}$$

We can extend the equation (2.5) to small variation of the power injected P_i^{dc} :

$$\sum_{i=1}^{N} \Delta P_i^{\mathrm{dc}} = 0 \tag{2.5}$$

with $\Delta P_i^{\mathrm{dc}} = P_i^{\mathrm{dc}} - P_i^{\mathrm{dc-ref}}$ where $P_i^{\mathrm{dc-ref}}$ represents the power reference injected from the AC area i to the DC grid for $f = f^{\mathrm{ref}}$ the reference value of the frequency of the area i. In this thesis the following initial conditions are considered : $P_i^{\mathrm{dc}}(0) = P_i^{\mathrm{dc-ref}}$ [5].

2.2.3 AC Area Model

Since the time scale of the primary frequency control is relatively small, the frequency is considered identical for the generators with in a AC area [5]. Therefore, based on [5] [24], the aggregation method is used to represent the mechanical model of the generators in the AC areas.

This method allows a replacement of a group of generators possessing similar characteristics by an equivalent generators model. The equivalent coefficients are calculated using structure preservation of the coefficient matrices expressing the dynamics followingwithin machines.

The parameters of the equivalent controller are found through a linear aggregation of each control system of the generators [24].

Therefore, for the AC area i, the aggregated dynamic of the frequency is expressed as :

$$2\pi J_i \frac{\mathrm{d}f_i}{\mathrm{d}t} = \frac{P_{\mathrm{mech}i} - P_{\mathrm{elec}i}}{2\pi f_i} - 2\pi D_{\mathrm{g}i}(f_i - f_i^{\mathrm{ref}}) \tag{2.6}$$

where f_i represents the frequency of the AC area i; f_i^{ref} represents the reference value of the frequency of the AC area i; $P_{\mathrm{mech}i}$ and $P_{\mathrm{elec}i}$ represent respectively the mechanical power input and the electrical power output of the aggregated generator of the AC area i; J_i represents the moment of inertia and $D_{\mathrm{g}i}$ the damping factor of the aggregated generator.

The power balance must be satisfied inside the AC area i. Therefore the electrical power output of the aggregated generator of the area i is defined as:

$$P_{\mathrm{elec}i} = P_{\mathrm{load}i} + P_i^{\mathrm{dc}} \tag{2.7}$$

with $P_{\mathrm{load}i}$ the load for the AC area i. To represent the load of the AC areas i, the static load model is used in this research [5] [25]:

$$P_{\mathrm{load}i} = P_{\mathrm{load}i}^{\mathrm{ref}}.(1 + Q_{\mathrm{l}i}(f_i - f_i^{\mathrm{ref}})) \tag{2.8}$$

where $P_{\mathrm{load}i}^{\mathrm{ref}}$ is the value of $P_{\mathrm{load}i}$ for $f_i = f_i^{\mathrm{ref}}$ and $Q_{\mathrm{l}i}$ is the frequency sensitivity factor.

2.2.4 Linearizion and Manipulation

The equation (2.1) and (2.6) needs to be reformulate in order for the system to be expressed as a set of state space equations:

$$\dot{\mathbf{x}} = A\mathbf{x} + B\mathbf{u}$$
$$\mathbf{y} = C\mathbf{x} \tag{2.9}$$

with $\mathbf{x} \in \mathbb{R}^n$ the state variables relative to the system, $\mathbf{y} \in \mathbb{R}^m$ the output of the system, $\mathbf{u} \in \mathbb{R}^r$ the input of the system, $A \in \mathbb{R}^{n\times n}$ the state matrix, $B \in \mathbb{R}^{n\times r}$ the control input matrix and $C \in \mathbb{R}^{m\times n}$ the output matrix.

2.2.4.1 Manipulation of the Dynamic Frequency Model

In order to derive the state space equations of the system we first linearize the equation (2.6) around the $f_i = f_i^{\text{ref}}$ which provides:

$$2\pi J_i \frac{\mathrm{d}f_i}{\mathrm{d}t} = \frac{P_{\text{mech}i} - P_{\text{load}i} - P_i^{\text{dc}}}{2\pi f_i^{\text{ref}}} - 2\pi Q_i(f_i - f_i^{\text{ref}}) \tag{2.10}$$

with $Q_i = D_{\text{g}i} + \frac{P_{\text{load}i}^{\text{ref}} Q_{\text{g}i}}{4\pi^2 f_i^{\text{ref}}}$ [5].

Then, we introduce a new sets of variables : $\Delta P_i^{\text{dc}} = P_i^{\text{dc}} - P_i^{\text{dc-ref}}$, $\Delta f_i = f_i - f_i^{\text{ref}}$, $\Delta P_{\text{mech}i} = P_{\text{mech}i} - P_{\text{mech}i}$ and $\Delta P_{\text{load}i} = P_{\text{load}i} - P_{\text{load}i}^{\text{ref}}$. The equation (2.1) and (2.10) are modified to express our system in function of these variables:

$$2\pi J_i \frac{\mathrm{d}f_i}{\mathrm{d}t} = \frac{P_{\text{mech}i} - P_{\text{load}i} - P_i^{\text{dc}}}{2\pi f_i^{\text{ref}}} - 2\pi Q_i(f_i - f_i^{\text{ref}}), \tag{2.11}$$

$$\frac{\mathrm{d}f_i}{\mathrm{d}t} = \frac{P_{\text{mech}i} - P_{\text{load}i} - P_i^{\text{dc}}}{4\pi^2 J_i f_i^{\text{ref}}} - \frac{Q_i}{J_i}(f_i - f_i^{\text{ref}}). \tag{2.12}$$

For $f_i = f_i^{\text{ref}}$, $P_{\text{mech}i} = P_{\text{mech}i}^{\text{ref}}$, $P_{\text{load}i} = P_{\text{load}i}^{\text{ref}}$, and $P_i^{\text{dc}} = P_i^{\text{dc-ref}}$. Therefore :

$$\frac{\mathrm{d}f_i^{\text{ref}}}{\mathrm{d}t} = \frac{P_{\text{mech}i}^{\text{ref}} - P_{\text{load}i}^{\text{ref}} - P_i^{\text{dc-ref}}}{4\pi^2 J_i f_i^{\text{ref}}} = 0. \tag{2.13}$$

We subtract the equation (2.13) to (2.12) in order to obtain:

$$\frac{\mathrm{d}f_i}{\mathrm{d}t} - \frac{\mathrm{d}f_i^{\mathrm{ref}}}{\mathrm{d}t} = \frac{P_{\mathrm{mech}i} - P_{\mathrm{load}i} - P_i^{\mathrm{dc}}}{4\pi^2 J_i f_i^{\mathrm{ref}}} - \frac{Q_i}{J_i}(f_i - f_i^{\mathrm{ref}}) - \frac{P_{\mathrm{mech}i}^{\mathrm{ref}} - P_{\mathrm{load}i}^{\mathrm{ref}} - P_i^{\mathrm{dc-ref}}}{4\pi^2 J_i f_i^{\mathrm{ref}}}. \tag{2.14}$$

Therefore:

$$\frac{\mathrm{d}\Delta f_i}{\mathrm{d}t} = \frac{\Delta P_{\mathrm{mech}i} - \Delta P_{\mathrm{load}i} - \Delta P_i^{\mathrm{dc}}}{4\pi^2 J_i f_i^{\mathrm{ref}}} - \frac{Q_i}{J_i}(\Delta f_i). \tag{2.15}$$

2.2.4.2 Manipulation of the Primary Frequency Control Model

From the equation (2.1) we know:

$$T_{\mathrm{mech}i}\frac{\mathrm{d}P_{\mathrm{mech}i}}{\mathrm{d}t} = P_{\mathrm{mech}i}^{\mathrm{ref}} - P_{\mathrm{mech}i} - \frac{P_i^{\mathrm{ref}}}{\sigma}\frac{f_i - f_i^{\mathrm{ref}}}{f_i^{\mathrm{ref}}}. \tag{2.16}$$

As previously, we consider $f_i = f_i^{\mathrm{ref}}$, $P_{\mathrm{mech}i} = P_{\mathrm{mech}i}^{\mathrm{ref}}$, $P_{\mathrm{load}i} = P_{\mathrm{load}i}^{\mathrm{ref}}$, and $P_i^{\mathrm{dc}} = P_i^{\mathrm{dc-ref}}$. Then:

$$\frac{\mathrm{d}P_{\mathrm{mech}i}^{\mathrm{ref}}}{\mathrm{d}t} = 0. \tag{2.17}$$

The equation (2.17) is subtracted to (2.16) and we obtain:

$$\frac{\mathrm{d}\Delta P_{\mathrm{mech}i}}{\mathrm{d}t} = \frac{-\Delta P_{\mathrm{mech}i}}{T_{\mathrm{mech}i}} - \frac{P_i^{\mathrm{ref}}}{\sigma T_{\mathrm{mech}i}}\frac{\Delta f_i}{f_i^{\mathrm{ref}}}. \tag{2.18}$$

3.0 OPTIMAL DISTRIBUTED CONTROL MODEL

This thesis considers a multiterminal HVDC system with N converters so N AC areas. Among these N converters, $N-1$ control the power exchange between the DC grid and the $N-1$ AC areas. The Nth converter is considered as a slack bus which regulate the DC voltage close to its reference value.

3.1 OPTIMAL CONTROL SYSTEM

3.1.1 Continuous LQR Optimization

The state-space system synthesizing the dynamics of the system is:

$$\begin{aligned} \dot{\mathbf{x}} &= A\mathbf{x} + B\mathbf{u} \\ \mathbf{y} &= C\mathbf{x} \end{aligned} \tag{3.1}$$

with $\mathbf{x} \in \mathbb{R}^n$ the state variables relative to the system, $\mathbf{y} \in \mathbb{R}^m$ the output of the system, $\mathbf{u} \in \mathbb{R}^r$ the input of the system, $A \in \mathbb{R}^{n\times n}$ the state matrix, $B \in \mathbb{R}^{n\times r}$ the control input matrix and $C \in \mathbb{R}^{m\times n}$ the output matrix.The system is regulated with a state feedback controller (Fig. 3.1) with $\mathbf{r} = 0$. Therefore :

$$\mathbf{u} = -K\mathbf{x} \tag{3.2}$$

with K the coefficients of the state feedback [17], [26].

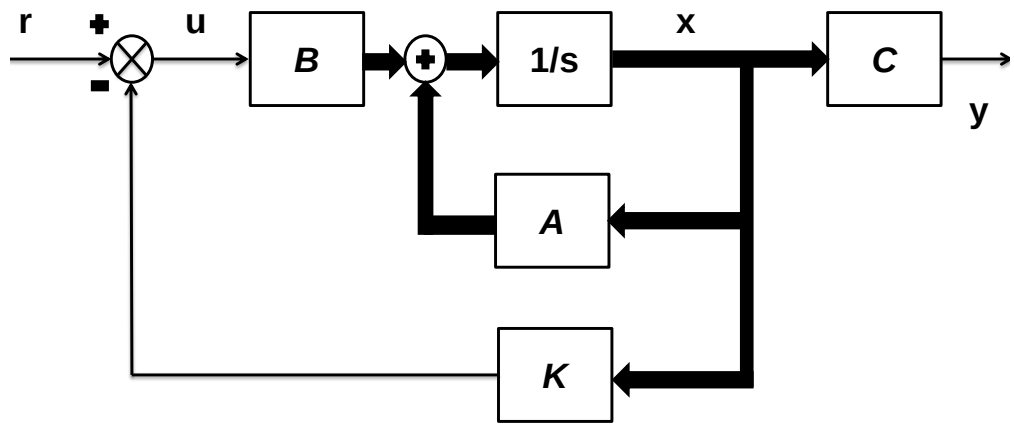

Figure 3.1: Classic representation state space regulator.

Based on this system model, we can derive the performance index :

$$J = \frac{1}{2}\int_0^\infty [\mathbf{x^T}(t)Q\mathbf{x}(t) + \mathbf{u^T}(t)R\mathbf{u}(t)]\ dt \tag{3.3}$$

with $Q \in \mathbb{R}^{n\times n}$ and $R \in \mathbb{R}^{r\times r}$ the weighting matrices of the quadratic performance expression. Q has to be symmetric and positive semi-definite ($Q \geq 0$) and R symmetric and positive definite ($R > 0$).

To find the optimal coefficient for the feedback controller, it is necessary to first solve the Riccati equation:

$$-\dot{S} = A^{\mathbf{T}}S + SA - SBR^{-\mathbf{1}}B^{\mathbf{T}}S + Q. \tag{3.4}$$

Then, based on the solution S of the Riccati equation, the optimal state feedback controller K is:

$$K = R^{-\mathbf{1}}B^{\mathbf{T}}S. \tag{3.5}$$

3.1.2 Distributed Control System

3.1.2.1 Optimal Frequency Control Model

This thesis considers a distributed control scheme using a Proportional-Integral-Derivative (PID) control with optimal coefficients for each $N-1$ sub-controllers. The sub-controller i is attributed to the converter i. Each sub-controller i controls the frequency excursion by modifying the power injected inside of the DC grid by the area i : $P_1^{\mathrm{dc}}, ..., P_{N-1}^{\mathrm{dc}}$. The value of P_N^{dc} is determined in order to maintain power injected balance inside the DC grid (2.5).

According to equation (2.15), $\Delta P_{\mathrm{mech}i}$ contains information about the derivative of Δf_i. In other words $\frac{\mathrm{d}\Delta f_i}{\mathrm{d}t} = f(\Delta P_{\mathrm{mech}i})$. Consequently, in order to design a PID controller, $\int \Delta f_i$, Δf_i and $\Delta P_{\mathrm{mech}i}$ needs to be the states variables of the system. Therefore, the sub-controller i is designed as :

$$\Delta P_i^{\mathrm{dc}} = \sum_{k=1}^{N} K_{ik}. \int \Delta f_k + \sum_{k=1}^{N} K_{pk}.\Delta f_k + \sum_{k=1}^{N} K_{dk}.\Delta P_{\mathrm{mech}k} \tag{3.6}$$

with $\Delta f_i = f_i - f_i^{\mathrm{ref}}$, $\Delta P_{\mathrm{mech}i} = P_{\mathrm{mech}i} - P_{\mathrm{mech}i}^{\mathrm{ref}}$ and K_p, K_i and K_d respectively the proportional, integral and derivative gain of the PID controller.

Intuitively the equation (3.6) is compatible with our goal. A small excursion of the frequency will automatically induce a modification of the power mechanical (equations (2.15) and (2.18)) which will induce a modification of the power injected inside the DC grid and therefore stabilize the frequency of the system. The optimization of the coefficients is centralized with the assumptions that all states of the system are accessible. We have therefore an optimal full states feedback regulator.

3.1.2.2 Frequency Control Model from [5]

In [5], the J.Dai proposed a distributed Proportional-Integral (PI) control scheme to control the interconnected AC areas. The $N-1$ sub-controllers control $P_1^{\mathrm{dc}}, ..., P_{N-1}^{\mathrm{dc}}$. The value of P_N^{dc} is determined in order to maintain power injected balance inside of the DC grid (2.5).

The *rendez-vous* method is used to design the sub-controller. This method is based a consensus protocol between a number of agents x_i called consensus average or nearest neighbor rules:

$$\dot{x}_i = -\sum_{j \in N_i} (x_i - x_j) \quad i \in \{1, ..., N\}. \tag{3.7}$$

The consensus average ensure that :*as long as the graph stays connected, the consensus equation drives all agents to the same state value*:

$$\lim_{t \to \infty} x_i(t) = \frac{1}{N} \sum_{j=1}^{N} x_{ij}(0) \quad i \in \{1, ..., N\}. \tag{3.8}$$

If each agent x_i contains the frequency of the AC area i, this method ensures that all AC areas share their primary reserves through the DC grid since the frequencies are linked through the consensus average. Therefore the $N-1$ sub-controllers are defined as :

$$\frac{\mathrm{d}P_i^{\mathrm{dc}}}{\mathrm{d}t} = \lambda_1 \sum_{j=1}^{N} b_{ij}(\Delta f_i - \Delta f_j) + \lambda_2 \sum_{j=1}^{N} b_{ij}(\frac{\mathrm{d}f_i}{\mathrm{d}t} - \frac{\mathrm{d}f_j}{\mathrm{d}t}) \tag{3.9}$$

with λ_1, λ_2 respectively the integral and proportional gain of the PI controller and b_{ij} are the graph communication coefficients of the AC areas. The value of b_{ij} is equal to 1 if the sub-controller i receives frequency information from the sub-controller j. Otherwise, it is equal to 0. For all the $N-1$ sub-controllers, the coefficients λ_1 and λ_2 in the controller are constant and equal.

3.2 MULTITERMINAL HVDC CONTROL MODEL

3.2.1 Substitution of the Variables

To facilitate the expression of the equations (2.15), (2.18) and (3.6) in a format of the state space equations we proceed to change the variables :

$$\mathbf{x}_i^{(1)} = \Delta f_i \quad \mathbf{x}_i^{(2)} = \int \Delta f_i \quad \mathbf{x}_i^{(3)} = \Delta P_{\text{mech}i}. \tag{3.10}$$

ΔP_i^{dc} is defined as the input of system $\mathbf{u}_i$, and $\Delta P_{\text{load}i}$ as the perturbation of the system $\mathbf{z}_i$. Therefore the equation (2.15) becomes :

$$\frac{\mathrm{d}\Delta f_i}{\mathrm{d}t} = \frac{\Delta P_{\text{mech}i} - \Delta P_{\text{load}i} - \Delta P_i^{\text{dc}}}{4\pi^2 J_i f_i^{\text{ref}}} - \frac{Q_i}{J_i}(\Delta f_i), \tag{3.11}$$

$$\frac{\mathrm{d}\mathbf{x}_i^{(1)}}{\mathrm{d}t} = \frac{\mathbf{x}_i^{(3)} - \mathbf{z}_i - \mathbf{u}_i}{4\pi^2 J_i f_i^{\text{ref}}} - \frac{Q_i}{J_i}(\mathbf{x}_i^{(1)}). \tag{3.12}$$

The same manipulation is made with the equation (2.18) which becomes :

$$\frac{\mathrm{d}\Delta P_{\text{mech}i}}{\mathrm{d}t} = \frac{-\Delta P_{\text{mech}i}}{T_{\text{mech}i}} - \frac{P_i^{\text{ref}}}{\sigma T_{\text{mech}i}} \frac{\Delta f_i}{f_i^{\text{ref}}}, \tag{3.13}$$

$$\frac{\mathrm{d}\mathbf{x}_i^{(3)}}{\mathrm{d}t} = \frac{-\mathbf{x}_i^{(3)}}{T_{\text{mech}i}} - \frac{P_i^{\text{ref}}}{\sigma T_{\text{mech}i}} \frac{\mathbf{x}_i^{(1)}}{f_i^{\text{ref}}}. \tag{3.14}$$

3.2.2 Substitution of the Parameters

In order to formulate the equations (3.12) and (3.14) in a matrix form compatible with the state space equations, the following parameters based on the equation (3.12) and (3.14) are defined [5] :

$$\alpha_{1,i} = \frac{Q_i}{J_i} \quad \alpha_{2,i} = \frac{1}{4\pi^2 f_i^{\text{ref}} J_i} \quad \alpha_{3,i} = \frac{P_i^{\text{ref}}}{T_{\text{mech}i}\sigma_i f_i^{\text{ref}}} \quad \alpha_{4,i} = \frac{1}{T_{\text{mech}i}}. \tag{3.15}$$

Consequently the equation (3.12) and (3.14) become:

$$\frac{\mathrm{d}\mathbf{x}_i^{(1)}}{\mathrm{d}t} = -\alpha_{1,i}\mathbf{x}_i^{(1)} + \alpha_{2,i}\mathbf{x}_i^{(3)} - \alpha_{2,i}\mathbf{u}_i - \alpha_{2,i}\mathbf{z}_i, \tag{3.16}$$

$$\frac{\mathrm{d}\mathbf{x}_i^{(3)}}{\mathrm{d}t} = -\alpha_{3,i}\mathbf{x}_i^{(1)} + \alpha_{4,i}\mathbf{x}_i^{(3)}. \tag{3.17}$$

The equation (3.17) represent the dynamics of the primary frequency control of the aggregated generator model.

To ensure that the steady state error is compensated, the secondary frequency control is necessary. In this thesis the dynamics of the secondary frequency control are synthesized by adding a term $-\beta\mathbf{x}_i^{(2)}$ in the equation (3.17).

This term represents the effect of the secondary frequency control on the evolution of the mechanical power $P_{\mathrm{mech}i}$. Therefore the equation (3.17) becomes:

$$\frac{\mathrm{d}\mathbf{x}_i^{(3)}}{\mathrm{d}t} = -\alpha_{3,i}\mathbf{x}_i^{(1)} + \alpha_{4,i}\mathbf{x}_i^{(3)} - \beta\mathbf{x}_i^{(2)}. \tag{3.18}$$

3.2.3 Formalization of the State Space Model

Since the main equations are in the good format, a generalization can be made for these equations in order to synthesize the whole multiterminal HVDC in one set of state space equations.

First, one details needs to be underline. From the equation (2.5) we know that the DC grid is considered lossless. In another word :

$$\sum_{i=1}^{N} \Delta P_i^{\mathrm{dc}} = \sum_{i=1}^{N} \mathbf{u}_i = 0. \tag{3.19}$$

As it was stipulated previously, we consider a multiterminal HVDC interconnected with N AC areas via N converters. The Nth controller has the role of a slack bus. It adjusts its power injected P_N^{dc} to ensure the balance within the DC grid. In other word :

$$\Delta P_N^{\mathrm{dc}} = \mathbf{u}_N = -\sum_{i=1}^{N-1} \Delta P_i^{\mathrm{dc}} = -\sum_{i=1}^{N-1} \mathbf{u}_i. \tag{3.20}$$

We define the following matrices :

$$A_k = \mathrm{diag}(\alpha_{k,1}, ..., \alpha_{k,N}) \in \mathbb{R}^{N\times N} \text{ for } k \in \{1, ..., 4\} \quad A_5 = \mathrm{diag}(\beta, ..., \beta) \in \mathbb{R}^{\mathrm{N}\times\mathrm{N}}, \tag{3.21}$$

$$A_6 = \begin{bmatrix} -\mathrm{diag}(\alpha_{2,1}, ..., \alpha_{2,N-1}) \\ \alpha_{2,N} \ ... \ \alpha_{2,N} \end{bmatrix} \in \mathbb{R}^{N\times N}, \tag{3.22}$$

$$I_N = \text{ Identity matrix } \in \mathbb{R}^{N\times N}. \tag{3.23}$$

The system of state space equations (3.1) becomes for a multiterminal HVDC interconnected with N AC areas :

$$\begin{aligned} \dot{\mathbf{x}} &= \begin{bmatrix} -A_1 & 0 & A_2 \\ I_N & 0 & 0 \\ -A_3 & -A_5 & -A_4 \end{bmatrix} \mathbf{x} + \begin{bmatrix} -A_6 \\ 0 \\ 0 \end{bmatrix} \mathbf{u} + \begin{bmatrix} -A_2 \\ 0 \\ 0 \end{bmatrix} \mathbf{z} \\ \mathbf{y} &= I_{3N}\mathbf{x}. \end{aligned} \tag{3.24}$$

The states variables of the system are :

$$\mathbf{x} = [\Delta f_1 ... \Delta f_N \ \int \Delta f_1 ... \int \Delta f_N \ \Delta P_{\mathrm{mech1}} ... \Delta P_{\mathrm{mech}N}]^T \in \mathbb{R}^{3N\times 1}, \tag{3.25}$$

$$\mathbf{x} = [\mathbf{x}_1^{(1)} ... \mathbf{x}_N^{(1)} \ \mathbf{x}_1^{(2)} ... \mathbf{x}_N^{(2)} \ \mathbf{x}_1^{(3)} ... \mathbf{x}_N^{(3)}]^T = [\mathbf{x}^{(1)} \ \mathbf{x}^{(2)} \ \mathbf{x}^{(3)}]^T \in \mathbb{R}^{3N\times 1}. \tag{3.26}$$

The inputs $\mathbf{u}$ and the external perturbations $\mathbf{z}$ of the system are respectively $\mathbf{u} = \begin{bmatrix} \mathbf{u}_1 \\ \vdots \\ \mathbf{u}_N \end{bmatrix} \in \mathbb{R}^{N\times 1}$ and $\mathbf{z} = \begin{bmatrix} \mathbf{z}_1 \\ \vdots \\ \mathbf{z}_N \end{bmatrix} \in \mathbb{R}^{N\times 1}$.

3.2.4 Optimal Feedback Control Applied to the System

We want to apply the optimal state feedback technique to find the optimal K . Therefore the system is considered in steady state operation with no external the perturbations $z = 0_N$. The system becomes :

$$\begin{aligned}\dot{\mathbf{x}} &= \begin{bmatrix} -A_1 & 0 & A_2 \\ 1_N & 0 & 0 \\ -A_3 & -A_5 & -A_4 \end{bmatrix} \mathbf{x} + \begin{bmatrix} -A_6 \\ 0 \\ 0 \end{bmatrix} \mathbf{u} \\ \mathbf{y} &= I_{3N}\mathbf{x}. \end{aligned} \tag{3.27}$$

We apply the different steps describe in the subsection 3.1.1 to find the optimal K. Depending on the values of the weights matrices Q and R the minimization of the cost function will not give the same result.

The matrix Q has an impact on the minimization of the state $\mathbf{x}$.The term $\mathbf{x^T}Q\mathbf{x}$, Q influences each state $(\mathbf{x}_i^{(k)})^2$ and the interaction between each state $\mathbf{x}_i^{(k1)}\mathbf{x}_j^{(k2)}$ with $k, k1, k2 \in \{1, 2, 3\}$ and $i \neq j$.

From a physical point of view it would not be accurate to look at the interaction between $\mathbf{x}_i^{(k1)}$ and $\mathbf{x}_i^{(k2)}$ for $k1 \neq k2$ since they have two totally different physical meanings. Therefore, we consider the matrix Q :

$$Q = \begin{bmatrix} Q_{11} & Q_{12} & Q_{13} \\ Q_{21} & Q_{22} & Q_{23} \\ Q_{31} & Q_{32} & Q_{33} \end{bmatrix} \in \mathbb{R}^{3N\times 3N} \text{ for } \mathbf{x} = [\mathbf{x}^{(1)}\ \mathbf{x}^{(2)}\ \mathbf{x}^{(3)}]^T \in \mathbb{R}^{3N\times 1}. \tag{3.28}$$

To ensure only the state itself and the interaction between states with the same physical meaning are considered in the minimization, we define :

$$Q_{12} = Q_{13} = Q_{21} = Q_{23} = Q_{31} = Q_{32} = 0_N. \tag{3.29}$$

id est, Q is a bloc diagonal matrix. In Q_{11}, Q_{22} and $Q_{33} \in \mathbb{R}^{N\times N}$, the values of the coefficients are important. Actually, the system accentuates the minimization of the corresponding states and interaction between states. The matrix R has an impact on the minimization of the input of the system $\mathbf{u}$. From the term $\mathbf{u^T}R\mathbf{u}$, R influences each input itself $(\mathbf{u}_i)^2$ and the interaction between each input $\mathbf{u}_i\mathbf{u}_j$ with $i \neq j$. Q and R designed and the system is defined, according to the equation (3.4), the Riccati equation can be solved to find S. It is then replaced it in the equation (3.5) to find the optimal controller K. We consider now the apparition of a variation of the load in or multiple areas. Therefore, under the optimal state space feedback the system becomes:

$$\begin{aligned} \dot{\mathbf{x}} &= (A - BK)\mathbf{x} + B_{new}\mathbf{z} \\ \mathbf{y} &= C\mathbf{x} \end{aligned} \tag{3.30}$$

where $\mathbf{z}$ is the variation of the load $\Delta P_{\text{load}i}$ and $B_{new} = \begin{bmatrix} -A_2 \\ 0 \\ 0 \end{bmatrix} \in \mathbb{R}^{N\times 1}$.

We can then easily study the outputs of the system under the perturbation regulated by the optimal state feedback designed previously.

4.0 RESULTS AND DISCUSSION

4.1 SIMULATION - BENCHMARK MULTITERMINAL HVDC

This section presents the different simulations applied to a benchmark system organized with five terminal HVDC system interconnected with five AC areas.This systems is studied under the distributed controller proposed in [5] and the optimal distributed controller presented in this thesis.

4.1.1 DC Grid Topology Parameters

The simulation considers a benchmark multiterminal HVDC system connected with five AC areas. The terminal or converter number 5 is designed as the slack bus of the AC-DC grid. The DC voltage is set at 100 kV. The topology of the multiterminal HVDC system is presented in the figure (4.1).

The communication between the terminals coincide with the physical lines of the DC grid. The admittance matrix Adm of the DC grid is defined as [5]:

$$Adm = \begin{bmatrix} 0.9592 & -0.7194 & 0 & 0 & -0.2398 \\ -0.7194 & 1.223 & -0.3597 & 0 & -0.1439 \\ 0 & -0.3597 & 0.7194 & -0.3597 & 0 \\ 0 & 0 & -0.3597 & 0.7194 & -0.3597 \\ -0.2398 & -0.1439 & 0 & -0.3597 & 0.7434 \end{bmatrix}. \tag{4.1}$$

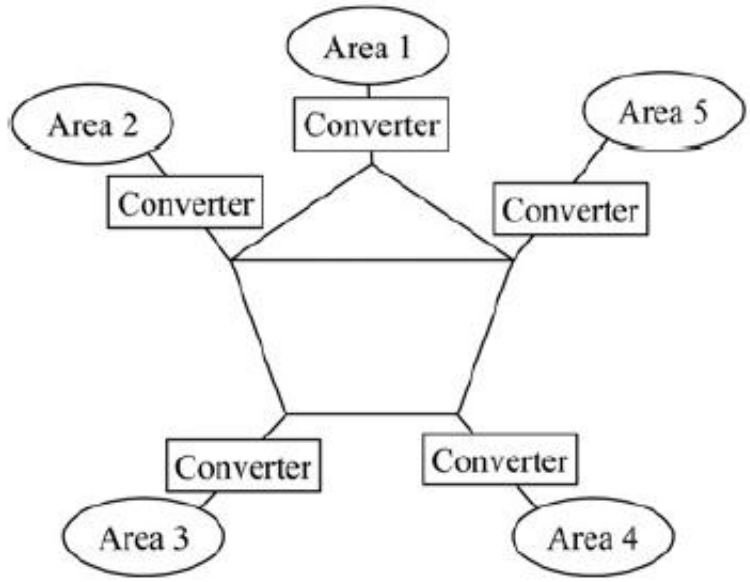

Figure 4.1: Topology of the multiterminal HVDC system [5].

4.1.2 AC Areas Parameters

The five AC areas are defined with the parameters and the initials values of the table (4.1). Two controllers will be tested to regulate the frequencies of the AC areas interconnected with the multiterminal HVDC : the distributed controller described in [5] presented in the section 3.1.2.2; and the optimal distributed controller derived in this research.

In the distributed control from [5] the non-linear differential equations the systems are integrated using the Euler's method. The sample step is fixed at $1ms$. The parameters of the PI controller λ_1, λ_2 are fixed to 2.10^6.

The simulation considers that the system initially operates under initial condition under steady state operation with $f_i = f_i^{\text{ref}} = 50Hz$. At $t = 10s$, a external perturbation is intro-

Table 4.1: Initial values and parameters for the AC areas [5]

	Area					Unit
	1	2	3	4	5	
f_{nom}	50	50	50	50	50	Hz
P_m^o	50	80	50	30	80.4	MW
P_{nom}	50	80	50	30	80.4	MW
J	2026	6485	6078	2432	4863	kg m^2
D_g	48.4	146.4	140	54.7	95.1	W s^2
σ	0.02	0.04	0.06	0.04	0.03	(dimensionless)
T_{sm}	1.5	2.0	2.5	2	1.8	s
P_l^o	100	60	40	50	40	MW
D_l	0.01	0.01	0.01	0.01	0.01	s
$\bar{P}^{\text{dc}}$	−50	20	10	−20	40.4	MW
$\bar{V}^{\text{dc}}$	99.17	99.60	99.73	99.59	100	kV

duce in the AC area number 2 : ΔP_{load2}. Its value is 5% of the reference value $P_{\text{load2}}^{\text{ref}}$.

The small value of the perturbation is justified by the fact that the system is linearized around $f_i = f_i^{\text{ref}}$. Therefore, the linearized model is only valid for small variations around the operating point f_i^{ref}.

For the optimal distributed controller we define the weights matrices Q and R:

$$Q = \begin{bmatrix} Q_{11} & Q_{12} & Q_{13} \\ Q_{21} & Q_{22} & Q_{23} \\ Q_{31} & Q_{32} & Q_{33} \end{bmatrix} \text{ and } R = I_4, \tag{4.2}$$

$$\text{with } Q_{11} = Q_{22} = \begin{bmatrix} 4\times10^6 & 1\times10^6 & 1\times10^6 & 1\times10^6 & 1\times10^6 \\ 1\times10^6 & 4\times10^6 & 1\times10^6 & 1\times10^6 & 1\times10^6 \\ 1\times10^6 & 1\times10^6 & 4\times10^6 & 1\times10^6 & 1\times10^6 \\ 1\times10^6 & 1\times10^6 & 1\times10^6 & 4\times10^6 & 1\times10^6 \\ 1\times10^6 & 1\times10^6 & 1\times10^6 & 1\times10^6 & 4\times10^6 \end{bmatrix} \text{ and } Q_{33} = I_5.$$

The parameter β is fixed at 10^6. The high values of these parameters are justified since they need to be coherent with the units of the different states (frequency Hz - mechanical power MW or 10^6W).

Also the matrix Q has an impact on the transient frequency response of system. Consequently by increasing the value of the Q, the minimization of the corresponding states *id est* $\Delta f_i \to 0$ is accentuated which is the the goal of the controller.

4.2 RESULTS

This chapter presents the simulations realized with MATLAB. The results are explained and compared.

4.2.1 Results with the Distributed Controller from [5]

The first graph of the figure (4.2) represents the system frequency response under the distributed control presented in [5].

As it was expected, the control scheme does not handle the secondary control. It leaves in a steady state error in the frequency deviation output $\Delta f_{\text{error}} = 0.02\ Hz$. Since all the frequencies of the AC areas are modified through the consensus average, all the generators participate and share their primary reserves to compensate the perturbation of the load P_{load2}.

From the transient point of view, the maximum peak of the response is $\Delta f_2 = 0.14\ Hz$. The transient response is considered small compared to the reference frequency 50 Hz.

The first graph of the figure (4.3) shows the variation of the mechanical power of the 5 AC areas under the distributed controller. We can see that each area participates in compensating the frequency deviation. The area 2 has a main pick at $2.7 \times 10^6\ W$ and is stabilized at $6.68 \times 10^5\ W$. The area 1 stabilizes at $8.35 \times 10^5\ W$; the area 5 stabilizes at $8.39 \times 10^5\ W$; the area 3 stabilizes at $2.78 \times 10^5\ W$ and the area 4 stabilizes at $2.5 \times 10^5\ W$.

4.2.2 Results with the Optimal Distributed Controller

4.2.2.1 Optimal Control with the Weight Matrices Q and R

The second graph of the figure (4.2) represent the system frequency response under the optimal distributed control formulate in this research.

The control scheme is able to cancel the steady states error. The frequency deviation output is canceled after 90 Ss. Since all the frequencies of the AC areas are modified through the consensus problem, all the generators participate and share their primary reserve to compensate the perturbation of the load P_{load2}.

The Optimal $K \in \mathbb{R}^{N-1\times 3N}$ of the system is :

$$K = \left[\begin{array}{ccccc} 6.7839 \times 10^6 & -1.6228 \times 10^6 & -1.0205 \times 10^6 & -6.2265 \times 10^5 & -4.0850 \times 10^6 \\ -8.8270 \times 10^5 & 8.2474 \times 10^6 & -5.2219 \times 10^5 & -4.1624 \times 10^5 & -4.9868 \times 10^5 \\ -1.0484 \times 10^6 & -1.6215 \times 10^6 & 4.9637 \times 10^6 & -6.2519 \times 10^5 & -5.7850 \times 10^6 \\ -8.7462 \times 10^5 & -1.0466 \times 10^6 & -5.0552 \times 10^5 & 3.1838 \times 10^6 & -4.9393 \times 10^6 \end{array}\right|$$

$$\left|\begin{array}{ccccc} 2.0956\times10^5 & -8.1949\times10^4 & -1.4365\times10^5 & -8.2726\times10^4 & -1.3856\times10^5 \\ -2.7864\times10^4 & 4.1584\times10^4 & -7.3049\times10^4 & -5.5402\times10^4 & -1.6835\times10^5 \\ -3.2483\times10^4 & -8.0895\times10^4 & 6.8763\times10^5 & -8.3417\times10^4 & -1.9489\times10^5 \\ -2.7614\times10^4 & -5.2601\times10^4 & -7.0446\times10^4 & 4.2329\times10^5 & -1.6676\times10^5 \end{array}\right| \tag{4.3}$$

$$\left|\begin{array}{ccccc} -0.2925 & -0.0124 & 0.0056 & -0.0139 & 0.1247 \\ -0.0135 & -0.1484 & 0.0148 & 0.0306 & 0.2335 \\ -0.0224 & 0.0590 & -0.0529 & 0.0594 & 0.2429 \\ -0.0127 & 0.0307 & 0.0137 & -0.1451 & 0.2343 \end{array}\right] \in \mathbb{R}^{N-1\times 3N}.$$

From the transient point of view, the maximum peak of the response is $\Delta f_2 = 0.12\ Hz$. However, an overshoot appears in the frequency respond in the areas 4 et 3 of $\Delta f_3 = 0.0099\ Hz$ and $\Delta f_4 = 0.017\ Hz$. These overshoots are small compared to the reference frequency 50 Hz.

The second graph of the figure (4.3) demonstrates the variation of the mechanical power of the 5 AC areas under the optimal distributed controller. Each area participate in the frequency deviation though differently than the interaction with the distributed controller from [5]: The area 2 has a peak at $2.93\times10^6\ W$ and a stabilized value at $2.28\times10^6\ W$. The area 1 has a peak at $2.82\times10^5\ W$ and stabilizes at $9.07\times10^4\ W$; the area 5 has a peak at $4.78\times10^5\ W$ stabilizes at $2.26\times10^5\ W$; the area 3 has a peak at $4.11\times10^5\ W$ and stabilizes at 2.42×10^5 and finally the area 4 has a peak at $3.39\times10^5\ W$ and stabilizes at $1.58\times10^5\ W$.

4.2.2.2 Optimal Control with the Weight Matrices $10 \times Q$ and R

Figure (4.4) presents the frequency deviation output of the 5 areas and the evolution of their mechanical power under the optimal control design with the weigh matrix $Q_{new} = 10 \times Q$ and $R_{new} = R$.

$$K = \left[\begin{array}{ccccc} 1.9114 \times 10^7 & -6.3551 \times 10^6 & -5.5329 \times 10^6 & -2.3984 \times 10^6 & -8.7586 \times 10^6 \\ -2.8581 \times 10^6 & 2.4744 \times 10^7 & -1.5713 \times 10^6 & -1.3823 \times 10^6 & -1.0853 \times 10^7 \\ -3.7999 \times 10^6 & -5.1428 \times 10^6 & 1.6091 \times 10^7 & -1.9599 \times 10^6 & -1.3452 \times 10^7 \\ -2.8117 \times 10^6 & -3.4971 \times 10^6 & -1.4723 \times 10^6 & 9.4338 \times 10^6 & -1.0712 \times 10^7 \end{array}\right|$$

$$\left|\begin{array}{ccccc} 5.8409 \times 10^5 & -3.2185 \times 10^5 & -7.7540 \times 10^5 & -3.1835 \times 10^5 & -2.9742 \times 10^5 \\ -8.8569 \times 10^4 & 1.2449 \times 10^6 & -2.2107 \times 10^5 & -1.8398 \times 10^5 & -3.6559 \times 10^5 \\ -1.0786 \times 10^5 & -2.5391 \times 10^5 & 2.2487 \times 10^6 & -2.6246 \times 10^5 & -4.4993 \times 10^5 \\ -8.7299 \times 10^4 & -1.7593 \times 10^5 & -2.0576 \times 10^5 & 1.2552 \times 10^6 & -3.6088 \times 10^5 \end{array}\right|$$

$$\left|\begin{array}{ccccc} -1.9053 & -0.0276 & 0.0816 & -0.0330 & 0.5797 \\ 0.1359 & -1.3429 & 0.1792 & 0.2602 & 1.1637 \\ 0.1954 & 0.6288 & -0.7319 & 0.6330 & 1.4123 \\ 0.1370 & 0.2565 & 0.1702 & -1.3436 & 1.1620 \end{array}\right] \in \mathbb{R}^{N-1 \times 3N}.$$

As previously stated the frequency deviation due to the load perturbation is canceled. The frequencies of the 5 AC areas go back to their references f^{ref} after 70 s.

The maximum peak is no longer for the frequency of the area 2 since Δf_2 reach only 0.078 Hz and stabilize around 70 s. Instead, the frequency deviation of the area 3 reach a maximum peak at 0.09 Hz with a small overshoot at 0.01 Hz.The area 4 has a peak value at 0.07 Hz and also an overshoot around 0.01 Hz. Those deviations are also small compared to the reference frequency 50 Hz.

From the second graph of the figure (4.4) all areas participate to cancel the frequency deviation. The area 2 has a peak value at $1.55 \times 10^6\ W$ and stabilizes around $1.3 \times 10^6\ W$; the area 3 has a peak value at $9.9 \times 10^5\ W$ and stabilizes around $7.29 \times 10^5\ W$; the area 4 has a peak value at $6.01 \times 10^5\ W$ and stabilizes around $3.87 \times 10^5\ W$; the area 5 has a peak value at $5.63 \times 10^5\ W$ and stabilizes around $3.48 \times 10^5\ W$ and finally the area 1 has a peak value at $4.84 \times 10^5\ W$ and stabilize around $2.32 \times 10^5\ W$.

4.3 DISCUSSION

Based on the figures (4.2) and (4.3), comments and comparisons are made. Both control scheme fulfill their objectives:

- For the distributed controller from [5], the objective is to stabilize the frequency deviation with the cooperation of all the AC areas interconnected through the DC grid.

- For the optimal distributed control derived in this thesis, the objective is to stabilize and to cancel the frequency deviation with the cooperation of the AC areas. The cooperation is directly linked to the cost function of the optimization and especially to the weighing matrix.

From the transient point of view, the distributed control scheme from [5] has a slight better response than the optimal control scheme: Indeed, the frequency response possesses no overshoot. However the frequency peak values response's of the area 2 with the optimal distributed control scheme is marginally smaller : $\Delta f_2 = 0.12\ Hz$ instead of with the distributed control $0.14\ Hz$. The appearance of the overshoot can be explained by the fact that the steady state value in the optimal control scheme must be f^{ref}. Therefore it necessitates an additional integrator which may generate smalls overshoots. The transient response is still acceptable since it is relatively small compared to $50\ Hz$.

The values of the optimal coefficients of matrix K give us an indication about the dominant states in the system. Indeed, a state corresponding to a coefficient K_{ij} close to 0 might be considered negligible compared to the other states.

However, the sign of the coefficients are not taken into account since the absolute value of the coefficients $|K_{ij}|$ is only considered. Moreover, the units of the states must be included in the study and coherent with the value of the coefficients K_{ij} associated.

In our case, the first 5×10 coefficients, corresponding to the states Δf_i and $\Delta \int f_i$, are relatively high. Their values are justifiable because the states have relatively small values. Furthermore, the aim of the controller is to regulate the frequency deviation, in other words to minimize the states. By consequence they cannot be negligible.

The last 5×5 coefficients, corresponding to the states $\Delta P_{\text{mech}i}$ are close to 0. However they cannot be considered negligible since the states $\Delta P_{\text{mech}i}$ takes values in the account of 10^4 and 10^6. In fact, the coordination of the sharing of the primary reserve between the AC areas are directly linked to the states. Indeed, by increasing the values of the coefficient Q_{33}, corresponding to the states $\Delta P_{\text{mech}i}$, we accentuate the minimization of the the states. Therefore the peak value of the output mechanical power of the area 2 is decreasing . But the system still needs to be stabilized and balanced. So the output mechanical power of the other areas increases to satisfy the balance requirement, improving the cooperation of the primary reserve.

As it was said previously, a modification of the weighting matrices Q and R has a clear impact on the response of the system. To improve the transient response associated with a better cooperation between the AC areas, a certain modification of the Q matrix can fulfill these requirement.

Figure (4.4) present the output frequency deviation Δf and the output power mechanical ΔP_{mech} with $Q_{\text{new}} = 10 \times Q$. On one hand an increase of the coefficient corresponding to Δf_i and $\Delta \int f_i$ will reduce the transient response consequently. On the other hand the increase of the coefficient corresponding to the states $\Delta P_{\text{mech}i}$ will improve the sharing load.

Based on the results presented previously, transient response and cooperation have been improved: The maximum peak value of the frequency is reduced by 65%. The stabilized mechanical power participation in the area 1 is improved by 39%; the area 2 by 56%; the area 3 by 56%; the area 4 by 40.8% and finally the area 5 by 65%.

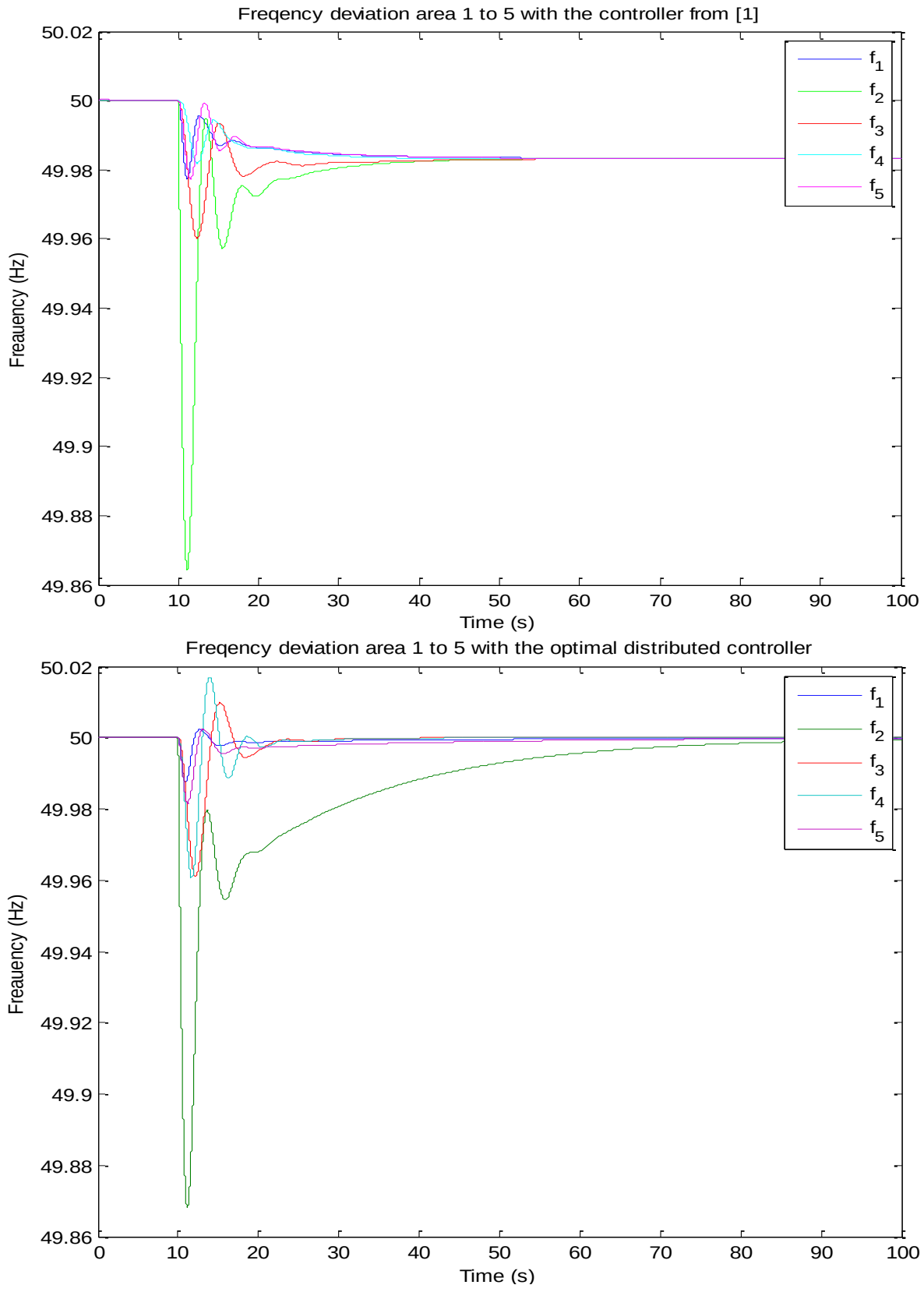

Figure 4.2: Frequency of the 5 areas with the controller from [5] and with the optimal distributed controller.

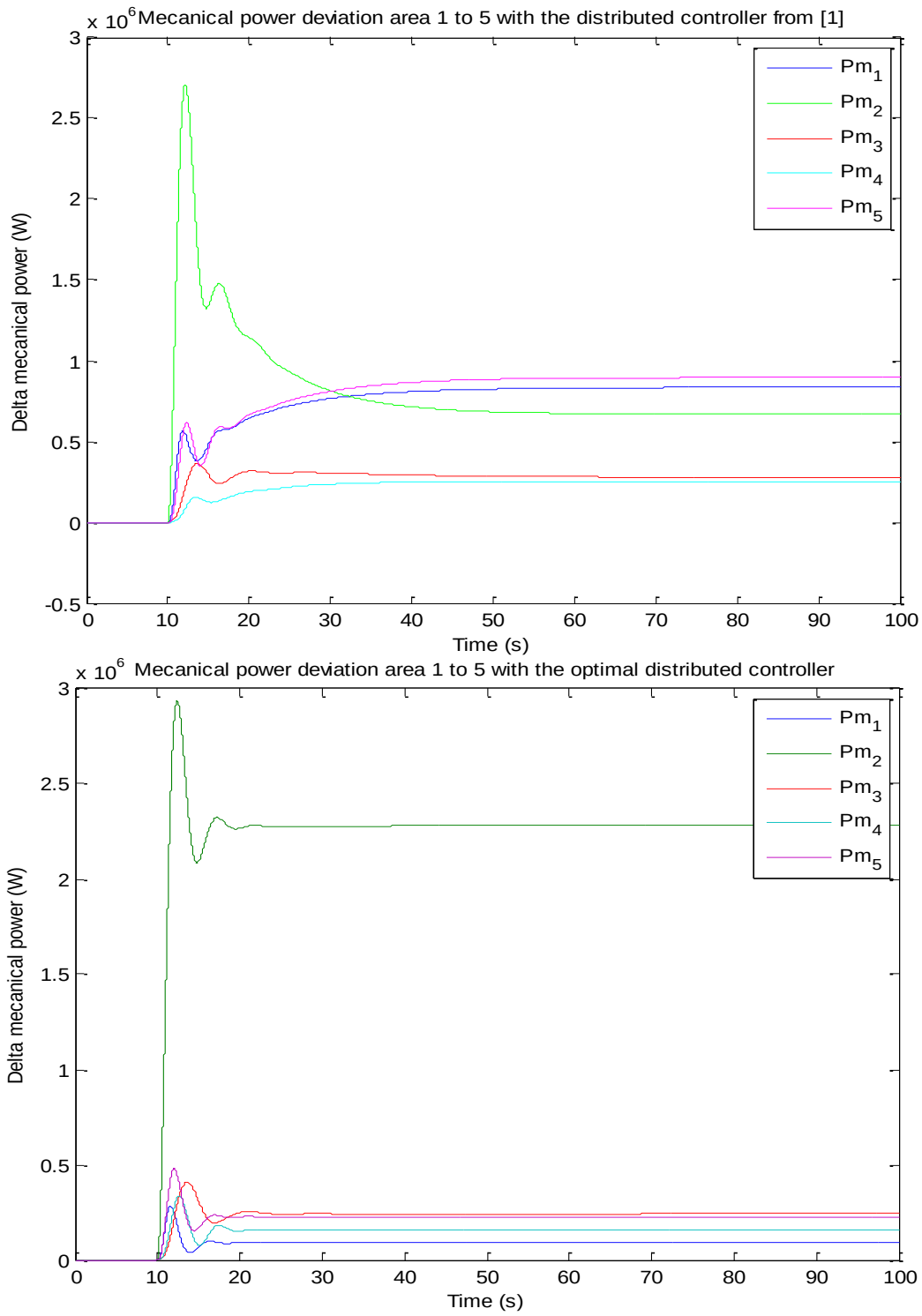

Figure 4.3: Mechanical power of the 5 areas with the distributed control from [5] and the optimal distributed controller.

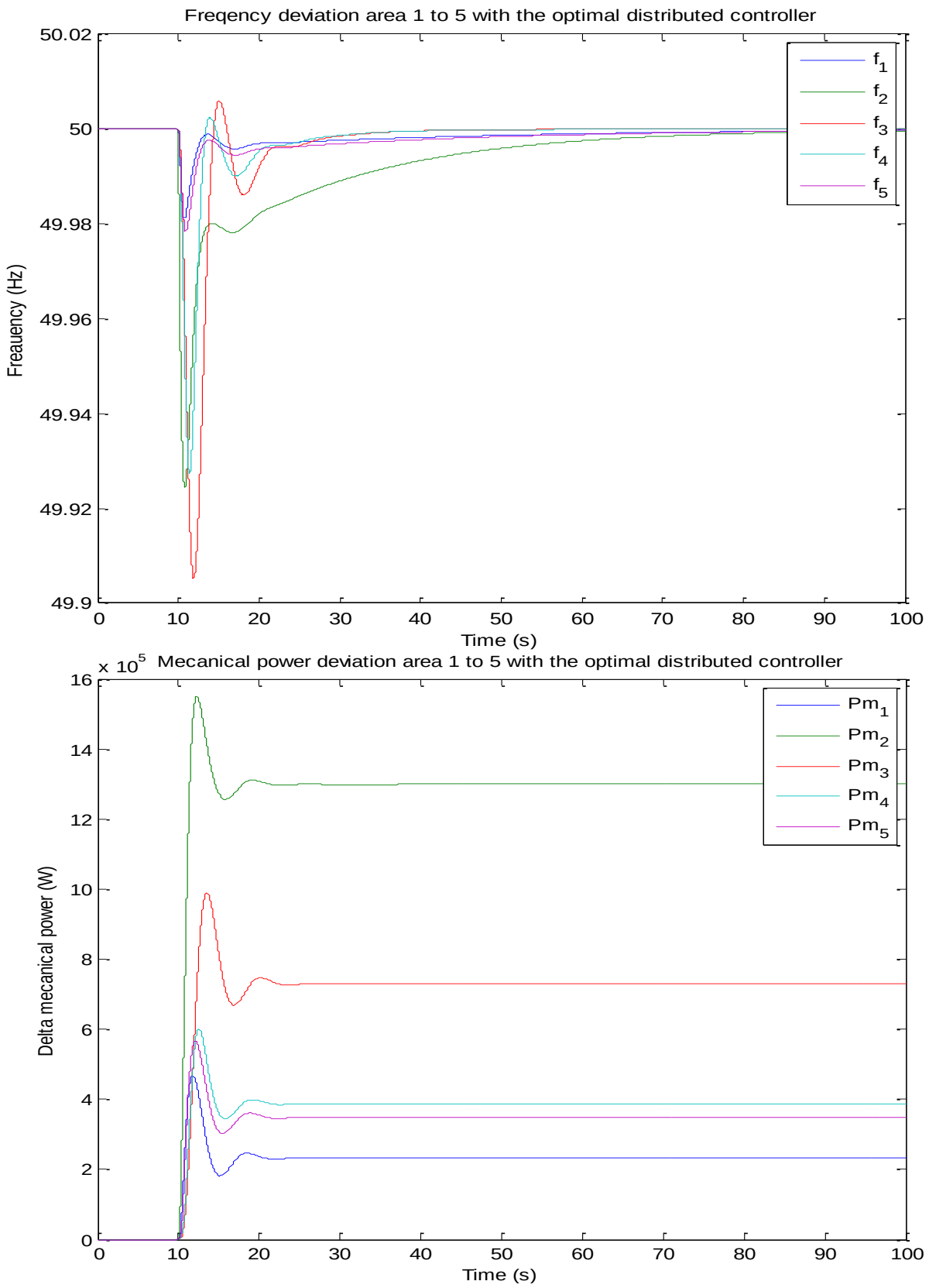

Figure 4.4: Frequency and power mechanical of the 5 areas with the optimal distributed controller.

5.0 CONCLUSIONS

This thesis presents the derivation of an optimal control design to regulate the frequency of multiterminal HVDC systems. The control scheme is synthesized with a PID controller through a state regulator, the parameters K_i, K_p and K_d are solved using the optimal control theory. The results are compared with those using the static PI controller from [5].

After the appropriate design of the weight matrices of the cost function, the results show an improvement as well as in the transient response than in the cooperation and collaboration between each AC area.

This is the first step toward the realization of a global optimal distributive controller for interconnected AC-DC areas. The communication topology of the DC grid must be taken into account within the optimization. A general optimization process to find the optimal topology coupled with the optimal control coefficients is the ultimate goal.

The design of this controller can be done using decentralized system and LMI (Linear Matrix Inequalities) theory to incorporate at the same time the optimizations coupled [27], [28] and [29].

BIBLIOGRAPHY

[1] M. P. Bahrman, "HVDC transmission overview," in *Transmission and Distribution Conference and Exposition, 2008. IEEE/PES*, pp. 1–7.

[2] A. Yazdani, R. Iravani, and MyiLibrary, "Voltage-sourced converters in power systems modeling, control, and applications," 2010.

[3] C. Du, E. Agneholm, and G. Olsson, "Comparison of different frequency controllers for a VSC-HVDC supplied system," *Power Delivery, IEEE Transactions on*, vol. 23, no. 4, pp. 2224–2232, 2008.

[4] P. Kundur, N. J. Balu, and M. G. Lauby, *Power system stability and control*. New York: McGraw-Hill, 1994.

[5] J. Dai, Y. Phulpin, A. Sarlette, and D. Ernst, "Coordinated primary frequency control among non-synchronous systems connected by a multi-terminal high-voltage direct current grid," *IET Generation Transmission and Distribution*, vol. 6, no. 2, pp. 99–108, 2012.

[6] J. Reeve, "Multiterminal HVDC power systems," *IEEE Transactions on Power Apparatus and Systems*, vol. PAS-99, no. 2, pp. 729–737, 1980.

[7] X. P. Zhang, "Multiterminal voltage-sourced converter-based HVDC models for power flow analysis," *IEEE Transactions on Power Systems*, vol. 19, no. 4, pp. 1877–1884, 2004.

[8] S. Cole, J. Beerten, and R. Belmans, "Generalized dynamic VSC MTDC model for power system stability studies," *IEEE Transactions on Power Systems*, vol. 25, no. 3, pp. 1655–1662, 2010.

[9] N. Rostamkolai, A. G. Phadke, W. F. Long, and J. S. Thorp, "An adaptive optimal-control strategy for dynamic stability enhancement of AC/DC power-systems," *IEEE Transactions on Power Systems*, vol. 3, no. 3, pp. 1139–1145, 1988.

[10] L. Xu and L. Yao, "DC voltage control and power dispatch of a multi-terminal HVDC system for integrating large offshore wind farms," *IET Renewable Power Generation*, vol. 5, no. 3, pp. 223–233, 2011.

[11] J. Liang, T. J. Jing, O. Gomis-Bellmunt, J. Ekanayake, and N. Jenkins, "Operation and control of multiterminal HVDC transmission for offshore wind farms," *IEEE Transactions on Power Delivery*, vol. 26, no. 4, pp. 2596–2604, 2011.

[12] X. Chen, H. S. Sun, J. Y. Wen, W. J. Lee, X. F. Yuan, N. H. Li, and L. Z. Yao, "Integrating wind farm to the grid using hybrid multiterminal HVDC technology," *IEEE Transactions on Industry Applications*, vol. 47, no. 2, pp. 965–972, 2011.

[13] W. Lu and B. T. Ooi, "Premium quality power park based on multi-terminal HVDC," *IEEE Transactions on Power Delivery*, vol. 20, no. 2, pp. 978–983, 2005.

[14] T. Nakajima and S. Irokawa, "A control system for HVDC transmission by voltage sourced converters," in *Power Engineering Society Summer Meeting, 1999. IEEE*, vol. 2, pp. 1113–1119 vol.2.

[15] L. Jun, O. Gomis-Bellmunt, J. Ekanayake, and N. Jenkins, "Control of multi-terminal VSC-HVDC transmission for offshore wind power," in *Power Electronics and Applications, 2009. EPE '09. 13th European Conference on*, pp. 1–10.

[16] L. Weixing and O. Boon-Teck, "DC overvoltage control during loss of converter in multi-terminal voltage-source converter-based HVDC (M-VSC-HVDC)," *IEEE Transactions on Power Delivery*, vol. 18, no. 3, pp. 915–920, 2003.

[17] M. S. Sachdev, R. J. Fleming, and J. Chand, "Optimal control of a HVDC transmission link," *Power Apparatus and Systems, IEEE Transactions on*, vol. PAS-92, no. 6, pp. 1958–1965, 1973.

[18] W. D. Yang, Z. Xu, and Z. X. Han, "Co-ordinated hierarchical control strategy for multi-infeed HVDC systems," *IEE Proceedings-Generation Transmission and Distribution*, vol. 149, no. 2, pp. 242–248, 2002.

[19] S. Lefebvre, D. CarrolL, and R. DeCarLo, "Decentralized power modulation of multiterminal HVDC systems," *IEEE Transactions on Power Apparatus and Systems*, vol. PAS-100, no. 7, pp. 3331–3339, 1981.

[20] C. Du, M. H. J. Bollen, E. Agneholm, and A. Sannino, "A new control strategy of a VSC-HVDC system for high-quality supply of industrial plants," *IEEE Transactions on Power Delivery*, vol. 22, no. 4, pp. 2386–2394, 2007.

[21] Z. Hongwei, F. L. Lewis, and Q. Zhihua, "Lyapunov, adaptive, and optimal design techniques for cooperative systems on directed communication graphs," *Industrial Electronics, IEEE Transactions on*, vol. 59, no. 7, pp. 3026–3041, 2012.

[22] O. Gomis-Bellmunt, J. Liang, J. Ekanayake, R. King, and N. Jenkins, "Topologies of multiterminal HVDC-VSC transmission for large offshore wind farms," *Electric Power Systems Research*, vol. 81, no. 2, pp. 271–281, 2011.

[23] G. Andersson, *Dynamics and Control of Electric Power Sytems.* Zurich, Switzerland: ETH, 2010.

[24] M. L. Ourari, L. A. Dessaint, and V. Q. Do, "Generating units aggregation for dynamic equivalent of large power systems," in *Power Engineering Society General Meeting, 2004. IEEE*, pp. 1535–1541 Vol.2.

[25] L. Grigsby, *Power system stability and control (The Electrical Engineering Handbool Series).* Boca Raton, USA: CRC Presse Inc, 2007.

[26] F. Lewis and V. Syrmos, *Optimal Control. Second Edition.* Wiley-Interscience Publication, John Wiley and Sons. Inc.

[27] C. Scherer, P. Gahinet, and M. Chilali, "Multiobjective output-feedback control via LMI optimization," *Automatic Control, IEEE Transactions on*, vol. 42, no. 7, pp. 896–911, 1997.

[28] D. D. Siljak, D. M. Stipanovic, and A. I. Zecevic, "Robust decentralized turbine/governor control using linear matrix inequalities," *Power Systems, IEEE Transactions on*, vol. 17, no. 3, pp. 715–722, 2002.

[29] D. D. iljak and A. I. Zeevi, "Control of large-scale systems: Beyond decentralized feedback," *Annual Reviews in Control*, vol. 29, no. 2, pp. 169–179, 2005.